Forced isoform switching of Neat1_1 to Neat1_2 leads to the hyperformation of paraspeckles but does not affect the development and growth of mice

Momo Isobe [1], Hikaru Toya [1], Mari Mito [2], Tomoki Chiba [3], Hiroshi Asahara [3], Tetsuro Hirose [4], and Shinichi Nakagawa [1*]

[1]RNA Biology Laboratory, Faculty of Pharmaceutical Sciences, Hokkaido University, Sapporo 060-0812, Japan
[2] RNA Systems Biochemistry Laboratory, RIKEN Cluster for Pioneering Research, 2-1 Hirosawa, Wako, Saitama 351-0198, Japan
[3]Department of Systems BioMedicine, Graduate School of Medical and Dental Sciences, Tokyo Medical and Dental University, Tokyo 113-8510, Japan
[4]Institute for Genetic Medicine, Hokkaido University, Sapporo 060-0815, Japan

*Correspondence should be addressed to

Shinichi Nakagawa
nakagawas@pharm.hokudai.ac.jp

Running title: Hyperformation of paraspeckles does not affect development

Abstract

Neat1 is a long non-protein coding RNA (lncRNA) that serves as an architectural component of nuclear bodies called paraspeckles. Two isoforms of Neat1, the short isoform Neat1_1 and the long isoform Neat1_2 are generated from the same gene locus by alternative 3' processing. Neat1_1 is expressed in various cell types, whereas Neat1_2 is expressed in a small population of particular cell types including the tip cells of the intestinal epithelium. To investigate the physiological significance of the isoform switching, we have created mutant mice that solely expressed Neat1_2 by deleting the upstream polyadenylation (poly-A) signal (PAS) required for the production of Neat1_1 (Neat1 ΔPAS). We observed the marked upregulation of Neat1_2 in various tissues and cells and the subsequent hyper-formation of paraspeckles, especially in cells that normally express Neat1_2. However, the mutant mice were born at normal Mendelian ratios and did not exhibit obvious external and histological abnormalities. These observations suggested that the hyperformation of paraspeckles does not interfere with the development and growth of these animals under normal laboratory conditions.

Introduction

A large number of long non-protein coding RNAs (lncRNA) are transcribed from the genome, and these transcripts regulate a variety of molecular and cellular processes including the epigenetic control of gene expression, mRNA processing, and the formation of nonmembranous cellular bodies (Long et al. 2017). Neat1 is one of the best-studied and functionally validated lncRNAs, and serves as an architectural component of nuclear bodies called paraspeckles (Fox et al. 2018). Paraspeckles are phase-separated nonmembranous nuclear bodies that are unique to mammalian species; more than 40 proteins assembled at a specific region of Neat1, forming a characteristic core-shell structure (Fox et al. 2018; Nakagawa et al. 2018). Paraspeckles have been proposed to function via the sequestration of paraspeckle-associated RNA binding proteins within these nuclear bodies (Hirose et al. 2014; Imamura et al. 2014). Two isoforms of Neat1, Neat1_1 (3.2 kb in mouse and 3.7 kb in human) and Neat1_2 (20 kb in mouse and 23 kb in human) are generated from the same locus by alternative 3' processing (Naganuma et al. 2012). Neat1_1 transcripts are processed by canonical 3' end processing complex CPSF6–NUDT21 (CFIm) and are cleaved at the polyadenylation (poly-A) signal (PAS) located upstream. The 3' processing of Neat1_1 is inhibited by Hnrnpk, which binds to sequences between the CFIm binding site and the PAS, resulting in the generation of readthrough products that give rise to the long isoform Neat1_2 (Naganuma et al. 2012; Yamazaki et al. 2018). The 3' end of Neat1_2 is cleaved by RNase P, and the non-polyadenylated transcripts are stabilized by triple-helix RNA structures found in the terminal region of Neat1_2 (Wilusz et al. 2012; Yamazaki et al. 2018). The specific knockdown of Neat1_2 leads to the disassembly of paraspeckles even in the presence of intact Neat1_1, suggesting that Neat1_2, but not Neat1_1, is required for the formation of paraspeckles (Sasaki et al. 2009). Whereas most of the cultured cell lines express both Neat1_1 and Neat1_2 and form paraspeckles, the strong expression of Neat1_2 is restricted to a subpopulation of particular cell types, while the expression of Neat1_1 is rather widespread (Nakagawa et al. 2011). Accordingly, prominent paraspeckle formations are found in only the small population of cells expressing high levels of Neat1_2, including the tip cells of the intestinal epithelium, the surface mucous cells of stomach, and the corpus luteal cells in the ovary

(Nakagawa et al. 2011). Cells that solely express Neat1_1 do not form paraspeckles, and Neat1_1 is diffusely localized to the nucleoplasm of these cells (Nakagawa et al. 2011; Li et al. 2017). Consistent with the strong expression of Neat1_2 in corpus luteal cells, the fertility of female Neat1 knockout (KO) mice is severely decreased due to the impaired formation of the corpus luteum and the subsequent decrease in serum progesterone (Nakagawa et al. 2014). Notably, only half of the Neat1 KO female mice exhibit a subfertile phenotype, and corpus luteal cells exhibit normal differentiation in the other half of the mutant mice, without the formation of paraspeckles. In addition, Neat1 can enhance or suppress cancer progression in a condition-specific manner (Adriaens et al. 2016; Mello et al. 2017). Paraspeckles are thus proposed to become essential only when mice are placed in certain environments, of which the precise molecular conditions have not been identified (Nakagawa et al. 2011; Nakagawa et al. 2014).

In this study, we forced the isoform switching of Neat1 by deleting the PAS required for the production of Neat1_1. Regardless of the hyperformation of paraspeckles in various tissues and cells, no overt phenotype was observed in the Neat1 ΔPAS mice. Our observation was consistent with the previous idea that paraspeckles are dispensable under normal laboratory conditions and function only when cells are placed in particular conditions.

Results

Neat1 ΔPAS mice were born at a normal Mendelian ratio

To generate an animal model that displayed forced isoform switching from Neat1_1 to Neat1_2, we created mutant mice that lacked the PAS of Neat1 using CRISPR/Cas9-mediated genome editing. To test the cleavage efficiency of multiple gRNAs, we initially transfected 3T3 cells with plasmids that express Cas9 nuclease and each gRNA targeting the region surrounding the Neat1 PAS (**Figure 1A**). Genomic DNA was isolated from the cells, and DNA fragments containing the cleavage site were amplified by PCR and subjected to a T7 endonuclease assay. Among the 5 gRNAs tested, one gRNA that cleaved the sequences inside the PAS (AATAAA) yielded the expected cleavage product at the highest efficiency (**Figure. 1B**). We then injected the in vitro-transcribed gRNA and Cas9 mRNA into fertilized eggs, and obtained 6 lines with various mutations (**Figure 1C**). We focused on a mutant line that lacked 39 nucleotides including the PAS, because it exhibited the highest expression of Neat1_2 relative to the expression of Neat1_1 in the salivary gland of heterozygous mice (**Figure 1D**). To confirm the lack of Neat1_1 expression, we prepared mouse embryonic fibroblast cells (MEFs) from wild-type and Neat1 ΔPAS embryos and performed Northern blot analyses using probes that detected both Neat1_1 and Neat1_2, and probes that specifically detected Neat1_2 (**Figure 2F**). The expression of Neat1_1 was completely lost in the Neat1 ΔPAS MEFs, whereas Neat1_2 was moderately upregulated in these cells (**Figure 1F**). The increase in Neat1_2 was also confirmed by in situ hybridization (**Figure 1G**), and the increase in Neat1_2 resulted in an increase in paraspeckle formation, as detected by the accumulation of the paraspeckle marker protein Nono (**Figure 1G, H**). The Neat1 ΔPAS mice were born at a normal Mendelian ratio (+/+:+/-:-/- =36:68:29 for males and 24:54:21 for females, $p = 1.00$ and 0.96, respectively, with a Chi-squared test), exhibited a normal body weight (wild-type = 23.9±2.4 g, KO = 24.3±3.6 g at 12-16 weeks, $p = 0.89$ with a Student's t-test), and had no overt morphological or behavioral defects.

Forced isoform switching by PAS deletion lead to the differential upregulation of Neat1_2 in each tissue

To confirm the isoform switching of Neat1_1 and Neat1_2 in various tissues, we performed Northern blot analyses using RNA prepared from each tissue (**Figure 2**). In all the cases, Neat1_1 expression was completely lost in Neat1 ΔPAS tissues, as was also the case in MEFs (**Figure 2B, D**). On the other hand, the upregulation of Neat1_2 was variable in different tissues (**Figure 2C, D**). For example, brown adipose tissue and intestinal tissue exhibited greater fold changes in Neat1_2, 4.12 and 3.9 fold, respectively (**Figure 2D**), whereas the testis and salivary gland exhibited much smaller fold changes, 1.88 and 1.82, respectively, compared to that in the respective wild-type tissues. This result was rather unexpected because the salivary gland expressed high levels of Neat1 and low levels of Neat1_2, and a forced isoform switch was anticipated to result in the abundant production of Neat1_2. We also noticed that the expression of Neat1_1 was almost absent in the liver (**Figure 2B**), which was not evident in previous in situ hybridization studies due to the lack of probes that specifically detected the short isoform (Nakagawa et al. 2011). The upregulation of Neat1_2 was evident when signals were detected with probes that specifically detected the long isoform (**Figure 2C**), but were much less evident with probes that simultaneously detected Neat1_1 and Neat1_2 (**Figure 2B**) for unknown technical reasons.

To study the isoform switching of Neat1 in the Neat1 ΔPAS mice and to study paraspeckle formations at the cellular level, we examined the expression of Neat1_1/2 and Neat1_2 by in situ hybridization in three representative tissues, the intestine, liver, and salivary gland (**Figures 3, 4**). In the intestine, the strong expression of Neat1_2 was restricted to the tip cells of the intestinal epithelium (**Figure 3A**), as previously described (Nakagawa et al. 2011). The areas that expressed Neat1_2 were expanded and included the middle region of the intestinal epithelium in the Neat1 ΔPAS mice (**Figure 3A**). The ectopic formation of paraspeckles in the middle region of the intestinal epithelium was confirmed by the colocalization of the paraspeckle marker proteins Sfpq and Nono (**Figure 4A-C**). Paraspeckle formation also increased in the tip cells in the intestinal epithelium, which normally form paraspeckles (**Figure 4A-C**). We also observed the enhanced expression of Neat1_2 and the subsequent hyperformation of paraspeckles in the liver (**Figure 3B, Figure 4A-C**), despite the lack of Neat1_1 expression based on a Northern blot (see discussion). In the salivary gland of wild-type mice, almost no signals was observed with probes that detected Neat1_2, and intense

signals were obtained in granular duct cells with probes that detected Neat1_1/2, suggesting that these cells almost exclusively expressed Neat1_1 (insets in **Figure 3C**). The signals obtained with the Neat1_1/2 probe were greatly reduced in the Neat1 ΔPAS mice (**Figure 3C**), which was consistent with the absence of Neat1_1 transcript signals on a Northern blot (**Figure 2B**). The increase in Neat1_2 expression (**Figure 3C**) and the formation of paraspeckles (**Figure 4A-C**) in the granular duct cells was not clear, as was the case in the tip cells of the intestinal epithelium or liver cells, suggesting that induced Neat1_2 produced by isoform switching cannot form paraspeckles in the granular duct cells. We examined the histology of the three tissues using hematoxylin and eosin (HE) staining, but no gross abnormalities were observed (**Figure 3A-C**).

To further investigate the formation of paraspeckles at a higher resolution, we observed paraspeckles using a structural illumination microscope (**Figure 4D**). The core-shell structure of paraspeckles that was previously described (West et al. 2016) was not evident in the tissue sections probably because of the freeze-thaw process that was performed during the preparation of the samples. However, paraspeckle formations were clearly recognizable by the accumulation of Neat1_2 and Nono, which made spherical structures in the cells that strongly expressed Neat1_2 (**Figure 4D**). In the salivary glands of Neat1 KO mice, Neat1_2 overlapped with Nono but did not form distinct paraspeckles with round shape (**Figure 4D**), suggesting that the assembly of Neat1 ribonucleoproteins was incomplete in this cell type.

In summary, Neat1_2 was differentially upregulated in the Neat1 ΔPAS mice, which did not correlate with the expression levels of Neat1_1, resulting in the differential hyperformation of paraspeckles in each cell type.

Not all of the paraspeckle proteins were ubiquitously expressed in mouse tissues

To obtain more insights into the molecular mechanisms driving the differential increase in Neat1_2 and paraspeckle formations in the Neat1 ΔPAS mice, we examined the expression pattern of a series of paraspeckle proteins in the intestine, liver, and salivary glands (**Figure 5**). For these experiments, we used freshly frozen sections without the simultaneous detection of Neat1 RNA to increase the sensitivity of the immunostaining, although the paraspeckle localization of these proteins became less clear due to higher nucleoplasmic signals.

To date, more than 40 paraspeckle proteins have been identified, and they are classified into 5 categories according to their function during the formation of paraspeckles (Naganuma et al. 2012; Kawaguchi et al. 2015). Category 1 proteins are essential for the formation of paraspeckles, and these proteins are further divided into two subcategories, Category 1A that regulate the production of Neat1_2 and Category 1B proteins, which assemble Neat1_2 ribonucleoprotein complexes. Category 2 proteins are partially required for the formation of paraspeckles, and the depletion of these proteins leads to the decreased formation of paraspeckles. Category 3 proteins do not affect the formation of paraspeckles; Category 3A proteins regulate the amount of the nonessential isoform Neat1_1; Category 3B proteins do not have any clear effect on the formation of paraspeckles or on the amount of Neat1. We performed immunostaining to detect Sfpq, Nono, and Hnrnpk (Category 1A); Fus and Brg1 (Category 1B); Tardbp (Category 2); Cpsf6 (Category 3A); and Pspc1 and Ewsr1 (Category 3B). All of these paraspeckle proteins exhibited strong expression in the intestinal epithelium irrespective of their positions within the tissue, suggesting that the cell-type specific expression of Neat1_2 and the formation of paraspeckles in the tip cells were regulated by other paraspeckle proteins and/or by the modification of the paraspeckle proteins that modulate their activities (**Figure 5A, B**). The ubiquitous expression of paraspeckle proteins was also observed in the liver, with the exception of Brg1, which exhibited weaker expression compared with that in the cells in other tissues (**Figure 5A, B**). On the other hand, the variable expression of paraspeckle proteins was observed in the granular duct cells that predominantly expressed Neat1_1 but that expressed much lower levels of Neat1_2; specifically, in most of the granular duct cells, the expression of Ewsr1 was almost absent, and the expression of Brg1, Hnrnpk, and Fus were greatly reduced, although the weak expression of these proteins was observed in a subpopulation of these cells (**Figure 5A, B**). Acinar cells, the majority of which do not normally express Neat1, expressed all of these paraspeckle proteins as well as Hnrnpk (an arrowhead in **Figure 5A**). The reduced expression of Hnrnpk was consistent with the lack of Neat1_2 expression in these cell types, as Hnrnpk induces isoform switching from Neat1_1 to Neat1_2 (Naganuma et al. 2012). To investigate whether different isoforms or modifications of paraspeckle proteins regulate the differential induction of Neat1_2 in Neat1 ΔPAS mice, we performed Western blot analyses using tissue lysates.

Although the expression levels of paraspeckle proteins were variable in each tissue, they exhibited similar migration patterns on Western blots except for Ewsr1 (**Figure 5C**).

Cellular differentiation of the intestinal epithelium and salivary gland were not altered in the Neat1 ΔPAS mice

Finally, we examined whether the molecular markers of cellular differentiation were altered in tissues that exhibited large changes in Neat1 expression in Neat1 ΔPAS mice. For these studies, we initially focused on the intestinal epithelium, where the ectopic formation of paraspeckles was clearly observed in the middle and bottom regions of the intestinal epithelium. The intestinal epithelium is composed of the following 5 different cell types, which can be identified by the expression of marker genes: multipotent stem cells that produce all of the cells in the intestinal epithelium (*Lgr5+* cells), Paneth cells that produce antimicrobial peptides (*Lyz1+* cells), goblet cells that secrete mucous (*Muc2+* cells), enteroendocrine cells that secrete intestinal hormones (*Chga+* cells), and enterocytes that are involved in nutrient uptake (Montgomery and Breault 2008)(**Figure 6A**). Enterocytes change their molecular properties as they are displaced towards the top of microvilli; bottom cells express high levels of *Cyb5r3* and *Pigr*, tip cells express high levels of *Apob*, and the top-most cells express *Nt5e* (Moor et al. 2018)(**Figure 6A**). All of these molecular markers exhibited similar expression patterns in Neat1 ΔPAS mice to those in wild-type mice (**Figure 6B**), suggesting that the organogenesis of the intestinal epithelium was not affected by the hyperformation of paraspeckles. We also examined the salivary gland, which strongly expressed Neat1_1, and Neat1_1 expression was completely lost in the salivary gland of mutant mice. The murine salivary gland is mainly composed of two cell types: acinar cells (Nkcc1+ cells) that secrete saliva (Evans et al. 2000), and granular duct cells that produce a number of growth factors and hormones, including NGF (Schwab et al. 1976) (**Figure 6C**). Again, we did not observe significant changes in the expression of these molecular markers in Neat1 ΔPAS mice (**Figure 6D**). Together, these results and the results of histological analyses using HE staining indicated that the deletion of the Neat1 PAS did not lead to observable phenotypes despite causing the hyperformation of paraspeckles and the loss of Neat1_1 expression.

Discussion

Here, we demonstrated that forced isoform switching by deletion of the Neat1 PAS leads to the loss of Neat1_1 and the concomitant upregulation of Neat1_2 in various mouse tissues, as was previously reported for U2OS cells (Li et al. 2017), HAP1 cells (Yamazaki et al. 2018), and ES cells (Modic et al. 2019). The ectopic formation of paraspeckles, as confirmed by the colocalization of Neat1_2 and the paraspeckle marker proteins Sfpq and Nono, was observed in the cells that normally do not express Neat1_2, including the middle cells in the intestinal epithelium. The enhanced formation of paraspeckles was also observed in cells that endogenously express Neat1_2, including the tip cells in the intestinal epithelium and in liver cells. Despite the hyperformation of paraspeckles in various cell types, Neat1 ΔPAS mice were born at normal Mendelian ratios and did not exhibit any obvious external or histological abnormalities. We also failed to detect any defects in cellular differentiation using the molecular markers that we tested. These observations were somewhat consistent with previous hypotheses that paraspeckles play essential roles when cells are placed under particular, and likely stressful conditions and are dispensable in normal laboratory conditions (Nakagawa et al. 2011; Nakagawa et al. 2014). Indeed, the expression of Neat1_2 and paraspeckle formation is enhanced by various stimuli, including viral infection (Saha et al. 2006), prolonged cell culture (Nakagawa et al. 2011), proteasome inhibition (Hirose et al. 2014), poly-I:C transfection (Imamura et al. 2014), and mitochondrial stress (Wang et al. 2018). Importantly, Neat1 is controlled by the p53 pathway, but cancer progression is enhanced or inhibited in a context-dependent manner: the lack of Neat1 enhances the development of premalignant pancreatic intraepithelial neoplasias in KrasG12D-expressing mice (Mello et al. 2017), whereas the progression of skin neoplasia induced by carcinogens is suppressed in Neat1 KO mice (Adriaens et al. 2016). It is therefore important to identify the precise molecular environment in which paraspeckles exert their function to further characterize the molecular function of Neat1 and of paraspeckles.

While previous studies demonstrated that the alternative use of the PAS results in the isoform switching of Neat1_1 and Neat1_2 (Naganuma et al. 2012; Li et al. 2017; Yamazaki et al. 2018; Modic et al. 2019), we noticed that the upregulation of

Neat1_2 was quite variable among tissues and did not correlate with the expression level of Neat1_1. For example, granular duct cells highly express Neat1_1, which should result in the abundant production of Neat1_2 in Neat1 ΔPAS mice. However, Neat1_2 is upregulated only moderately in these cells. As granular duct cells express a lower amount of Fus, which is essential for the assembly of Neat1 ribonucleoprotein complexes into paraspeckles (Naganuma et al. 2012; Shelkovnikova et al. 2014; West et al. 2016), the induced Neat1_2, which failed to form the nuclear bodies, might be less stable in this cell type. The impaired formation of paraspeckles in granular duct cells could also be explained by the decreased expression of other paraspeckle proteins, including Brg1, Hnrnpk, Pspc1, and Ewsr1. On the other hand, Neat1_2 is upregulated in the liver of Neat1 ΔPAS mice despite a lack of detectable expression of Neat1_1 on Northern blots, which cannot be explained by the isoform switching mechanism. We speculate that Neat1_1 is produced in liver cells but that it is unstable and is rapidly degraded, and the deletion of PAS may convert these cryptic Neat1_1 transcripts into stable Neat1_2, resulting in the enhanced formation of paraspeckles. Considering that Hnrnpk and Cpsf6 are ubiquitously expressed in mouse tissues, the ratio of Neat1_1 and Neat1_2 might be regulated by the differential stabilization of each isoform in certain cell types. Alternatively, the protein modification or differential isoforms of Hnrnpk and Cpsf6 might have differentially affected the selection of the Neat1 PAS. It will be important to investigate posttranscriptional regulation of Neat1 transcripts and the precise molecular features of the associating proteins to fully understand the physiological roles of paraspeckles and the molecular mechanisms that lead to the differential formation of paraspeckles in living organisms.

Materials and methods

Animals

All experiments were approved by the safety division of Hokkaido University (#2015-079). For anesthetization, medetomidine-midazolam-butorphanol (Kawai et al. 2011) was intraperitoneally injected at a volume of 10 µl/g of body weight. The genotyping of Neat1 ΔPAS mice were performed using Quick Taq HS DyeMix (Toyobo # DTM-101, Japan) and the following primers.

Neat1_PAS_KO_FW: 5'-GGGAAGCTGTTAAACTGTCAGTC-3'

Neat1_PAS_KO_RV: 5'-TCGGTATACAGGATGCTTTG-3'

The following PCR conditions were used: one cycle at 94ºC for 2 min; 35 cycles of 94ºC for 30 sec, 57ºC for 30 sec, and 68ºC for 1 min; followed by 68ºC for 5 min.

T7 endonuclease assay

To generate plasmid vectors expressing gRNAs designed targeting various regions around the Neat1 PAS, vectors were amplified with the following forward (F) and reverse (R) primers, and modified U6-expression vector was used as a template (Inui et al. 2014).

gRNA#1F: 5'-TCCCCTTTACAGCAAAATAAGTTTTAGAGCTAGAAATAGC-3'

gRNA#1R: 5'-TTATTTTGCTGTAAAGGGGACGGTGTTTCGTCCTTTCCAC-3'

gRNA#2F: 5'-TGCTGTAAAGGGGAGGAAAAGTTTTAGAGCTAGAAATAGC-3'

gRNA#2R: 5'-TTTTCCTCCCCTTTACAGCACGGTGTTTCGTCCTTTCCAC-3'

gRNA#3F: 5'-AGGGGAGGAAAATGGTTAGTGTTTTAGAGCTAGAAATAGC-3'

gRNA#3R: 5'-ACTAACCATTTTCCTCCCCTCGGTGTTTCGTCCTTTCCAC-3'

gRNA#4F: 5'-GAAGCTTCTTAGAATTGTCAGTTTTAGAGCTAGAAATAGC-3'

gRNA#4R: 5'-TGACAATTCTAAGAAGCTTCCGGTGTTTCGTCCTTTCCAC-3'

gRNA#5F: 5'-AAACCTTTATTTTGCTGTAAGTTTTAGAGCTAGAAATAGC-3'

gRNA#5R: 5'-TTACAGCAAAATAAAGGTTTCGGTGTTTCGTCCTTTCCAC-3'

After sequence validation, 3T3 cells were transfected with the gRNA-expressing plasmids and a Cas9-expressing plasmid hCas9 (Addgene #41815) using Lipofectamine LTX reagent (Thermo Fisher #15338100) following manufacturer's instructions. Genomic DNA was isolated using a standard procedure 65 hours after the transfection,

and DNA fragments around the target sequences were amplified with the following primers using Prime star max (Takara, Japan).

Neat1_T7_FW: 5'-GGGAAGCTGTTAAACTGTCAGTC-3'

Neat1_T7_RV: 5'-GACAGAATTGCATGTACAGACTG-3'

The following PCR conditions were used: 1 cycle at 98°C for 1 min; followed by 30 cycles of 10 sec at 94ºC, 10 sec at 55ºC, and 20 sec at 72ºC; and one cycle at 72ºC for 2 min.

Amplified fragments were purified using a Wizard SV Gel and PCR Clean-Up System (Promega #A9281), diluted at a concentration of 1 µg/20 µl, and subjected to denaturation-denaturation reactions with the following conditions: 1 cycle at 95ºC for 1 min and 60 cycles at 85ºC for 10 sec with a 1ºC decrease for each cycle; samples were then held at 25ºC. The reannealed fragments were treated with 5 units of T7 endonuclease 1 (NEB, #M0302S) at 37ºC for 25 min and immediately separated with 7% polyacrylamide gel electrophoresis.

Generation of genome-edited mice using RNA injection

To prepare template DNA for in vitro transcribed gRNA, PCR was performed using the following primers and the gRNA expression vector used for the T7 assay was used as a template.

Neat1_gRNA1_T7_temp FW:

5'-TAATACGACTCACTATAGGGGTCCCCTTTACAGCAAAATAA-3'

gRNA_Vec_RV:

5'-AAAAAAGCACCGACTCGGTG-3'

The following PCR conditions were used: 1 cycle at 94ºC for 2 min; followed by 30 cycles of 98ºC for 10 sec and 68ºC for 10 sec; and 1 cycle at 68ºC for 5 min. Amplified fragments were purified with QIAquick PCR Purification Kit (QIAGEN, #28104), and subjected to in vitro transcription using an mMESSAGE mMACHINE T7 Transcription Kit (Thermo Fisher #AM1344) following the manufacturer's instructions. Transcribed RNAs were purified with MEGAclea Transcription Clean-Up Kit (Thermo Fisher #AM1908). To prepare Cas9 mRNA, hCas9 was digested with NotI and purified with LiCl precipitation. In vitro transcription was performed using 1 µg of the template plasmid using an mMESSAGE mMACHINE T7 Transcription Kit, and the template

plasmid was digested with Turbo DNase (Thermo Fisher #AM2239). Transcribed mRNAs were purified using MEGAclea Transcription Clean-Up Kit and were used for injection. Single-stranded oligo-DNA was synthesized to introduce the EcoRV restriction site.

Neat1_EcoRV_ssDNA:
5'-TCGCACACGCTTCTCTGTACTAAAGTGTTCAGTGTACAAACCCACTAACCA
TTTTCCTCCCCTTTACAGCAAGATATCGGTTTGAGATTGAAGCTTCTTAGAATT
GTCATGGCTGTTACATTCTCGACCTCTGTCACTTTGCCTTCATAT-3'

The RNA and DNA were mixed with a concentration of 25 ng/µl Cas9 mRNA, 12.5 ng/µl gRNA, and 100 ng/µl ssDNA-oligo, and the injection into fertilized eggs was performed by RIKEN RRC. To identify genome-edited mice, genomic DNA was obtained from the tail of the mice using standard procedures, and PCR fragments were obtained using the primers for the T7 nuclease assay, and subjected to an agarose gel electrophoresis after digestion with EcoRV. The sequence of the amplified DNA fragments that exhibited differential migration was determined using direct sequencing.

qPCR analyses of Neat1_1/2 and Neat1_2 expression

RNA was obtained from mouse tissues using TRIzol reagent (Thermo Fisher # 15596026) following the manufacturer's instructions. To increase the recovery of Neat1_2, homogenized lysates were incubated at 55ºC for 5 minutes, as previously described (Chujo et al. 2017). cDNAs were synthesized with ReverTra Ace qPCR RT Master Mix (TOYOBO, # FSQ201), and qPCR was performed with a TAKARA Thermal Cycler Dice TP870 using TB Green Premix Ex TaqII (Takara #RR820A) and the following primers.

qPCR_Gapdh_FW: 5'-CCTCGTCCCGTAGACAAAATG-3'
qPCR_Gapdh_RV: 5'-TCTCCACTTTGCCACTGCAA-3'
qPCR_Neat1_1/2_FW: 5'-TTGGGACAGTGGACGTGTG-3'G
qPCR_Neat1_1/2_RV: 5'-TCAAGTGCCAGCAGACAGCA-3'
qPCR_Neat1_2_FW: 5'-GCTCTGGGACCTTCGTGACTCT-3'
qPCR_Neat1_2_RV: 5'-CTGCCTTGGCTTGGAAATGTAA-3'

Probe preparations for in situ hybridization

Neat1_1 and Neat1_2 were detected using probes that were described previously (West et al. 2016). For other markers, DNA fragments were prepared by RT-PCR as follows. To prepare cDNAs, 1 µg of total RNA was reverse transcribed using ReverTra Ace (TOYOBO # TRT-101) and oligo-dT (TOYOBO, # FSK-201) or random primers (TOYOBO # FSK-301) at 30ºC for 10 min, followed by 42ºC for 45 min, 50ºC for 15 min, and 99ºC for 5 min. Mixed cDNAs were used as a template for the subsequent PCR using PrimeSTAR Max DNA Polymerase (Takara # R045A). The following PCR conditions were used: 1 cycle at 98ºC for 1 min; 35 cycles at 98ºC for 10 sec, 55ºC for 5 sec, and 72ºC for 10 sec; followed by 72ºC for 1 min. Amplified fragments were purified using a Wizard SV Gel and PCR Clean-Up System and subcloned into pCRII using a TOPO TA Cloning™ Kit Dual Promoter (Thermo Fisher, # 450640). The following primers were used.

Chga_FW: 5'-ACACAGCCACCAATACCCAA-3'
Chga_RV: 5'-GTTATTGCAGTTGTGCCCCA-3'
Muc2_FW: 5'-GACCTGACAATGTGCCCAGA-3'
Muc2_RV: 5'-AGAAAACGGGGGCTAGAACG-3'
Lyz1_FW: 5'-TCGTTGTGAGTTGGCCAGAA-3'
Lyz1_RV: 5'-AGGCACAGCTCACTAGTCCT-3'
Lgr5_FW: 5'-ATGCGTTTTCTACGTTGCCG-3'
Lgr5_RV: 5'-GGTTGACTCACAGGACCGTT-3'
Nt5e_FW: 5'-CGATCGTCTACCTGGATGGC-3'
Nt5e_RV: 5'-GTTTCCCCTTACCCACTCCC-3'
Apob_FW: 5'-TCCAGAGAGTAGCCCGTGAT-3'
Apob _RV: 5'-AGTTCAGGCTGCTTTGAAGGT-3'
Pigr_FW: 5'-ATCTTCTGTGAGCTGCGACC-3'
Pigr_RV: 5'-CGTAACTAGGCCAGGCTTCC-3'
Cyb5r3_FW: 5'-GGTTGTTGGGGGAGCGG-3'
Cyb5r3_RV: 5'-GAGTTGGAAGGTGGTCCCTG-3'
Ngf_FW: 5'-GAGTTTTGGCCTGTGGTC-3'
Ngf_RV: 5'-TCGGTATACAGGATGCTTTG-3'
Nkcc1_FW: 5'-AGGTCTCTCTGTCGTCGTAA-3'
Nkcc1_RV: 5'-ATGGCCACAGATCATTAAAC-3'

To prepare a template for in vitro transcription, DNA fragments were amplified by PCR using M13 FW and RV primers and cDNAs that were subcloned into pCRII as a template. Amplified DNAs were purified with a Wizard SV Gel and PCR Clean-Up System and were used for in vitro transcription using Fluorescein RNA labeling Mix (Merck, # 11685619910) and T7 (Merck, # 10881767001) or SP6 polymerase (Merck, # 11487671001).

In situ hybridization and immunohistochemistry

In situ hybridization was performed as described previously (Nakagawa et al. 2011; Mito et al. 2016). Briefly, anesthetized adult mice were perfused with 4% paraformaldehyde (PFA) in PBS. Dissected tissues were further fixed for 16 hours at 4ºC, rinsed in PBS, and cryoprotected in 30% sucrose in PBS. After embedding in Tissue-Tek OCT compound (Sakura, Japan), frozen sections were cut at a thickness of 8 µm and were collected on poly-L-lysine (PLL)-coated slide glasses (Matsunami glass # S7441). After rehydration in PBS, the sections were subjected to in situ hybridization with Proteinase K treatment (Mito et al. 2016). MEF cells were cultured on a PLL-coated coverslips and fixed in 4% PFA in PBS, rinsed in PBS, permeabilized in 0.5% Triton X-100 for 10 min at room temperature, and processed for in situ hybridization without Proteinase K treatment (Mito et al. 2016). For immunohistochemistry, mice were perfused with 10 ml of PBS to reduce background signals from the endogenous IgGs, and dissected tissues were freshly frozen in OCT compound. Sections were fixed in 4% PFA overnight at 4ºC, and antigen retrieval was performed in HistoVT one (Nacalai, Japan, #06380) for 20 min in a Coplin jar placed in boiling water. The antigen retrieval treatment greatly reduces background signals derived from endogenous mouse IgG when using mouse monoclonal antibodies. The following antibodies were used: mouse monoclonal anti-Sfpq (Abcam, #ab11825), mouse monoclonal anti-Nono (Souquere et al. 2010), mouse monoclonal anti-Pspc1 (clone 1L4, Sigma), mouse monoclonal anti-Fus (clone 4H11, Santa Cruz), rabbit polyclonal anti-Brg1 (#A300-813A, Bethyl Laboratories), rabbit polyclonal anti-Tardbp (#10782-2-AP, Proteintech), Cy3-conjugated goat anti-mouse IgG (Merck, #AP124C), Alexa488-conjugated anti-rabbit IgG (Invitrogen, #A11029), and rabbit polyclonal anti-FITC (Abcam, #ab73831). To prepare paraffin-embedded sections, perfused tissues

were postfixed in Bouin's solution (Merck, # HT10132) for 16 hours at 4ºC and were processed using standard procedures. The fluorescent and bright field images were obtained using an epifluorescent microscope (BX51; Olympus) equipped with a CCD camera (DP70). Structural illumination microscopy images were obtained with a Zeiss PS1 microscope with a 63X water immersion objectives. The quantification of paraspeckle areas was performed by measuring the Neat1_2-positive areas that overlapped with Nono signals using ImageJ software.

Northern blotting

5 µg of total RNA was separated on a denaturing gel (1% agarose gel, 1X MOPS, 2% formaldehyde), and gels were rinsed twice in distilled water for 15 min, and RNAs were hydrolyzed in 0.05N NaOH for 20 min. This alkali treatment step is critical for detecting Neat1_2 transcripts. After soaking in water and subsequently soaking twice in 20X SSC 45 minutes, RNAs were transferred to a positively charged nylon membrane (Merck, #11209299001) and were hybridized with probes at a concentration of 1 µg/ml in DIG Easy hyb (Merck, #11603558001). Hybridized probes were detected with anti-Dig AP (Merck, # 11093274910) and CDP-star (Merck, # 11685627001) following the manufacturer's instructions.

Western blotting

5 µg of total proteins were separated on a precast 10-20% gradient gel (Funakoshi, #291M) and blotted on a nitrocellulose membrane using a semi-dry blotter following a standard protocol. Antibodies were diluted in Can Get Signal Immunoreaction Enhancer Solution (Toyobo, NKB-101) and detected with ECL prime (GE Healthcare, #RPN2232).

Acknowledgments

This work was supported by JSPS KAKENHI Grant Number 17H03604, 16H06279, 16H06276, MEXT KAKENHI Grant Number 26113005, and a Toray Science and Technology Grant granted to S.N., and a grant of the Joint Research Program of IGM, Hokkaido University to S.N. and T.H.

Author contributions: M.I. and H.T. performed immunostaining, in situ hybridization, and Western blot analyses, M.M., T.C., and H.A. designed and created the mutant mice, T.H. and S.N. designed the experiments, and S.N. wrote the paper with contributions from all authors.

References

Adriaens C, Standaert L, Barra J, Latil M, Verfaillie A, Kalev P, Boeckx B, Wijnhoven PW, Radaelli E, Vermi W et al. 2016. p53 induces formation of NEAT1 lncRNA-containing paraspeckles that modulate replication stress response and chemosensitivity. *Nat Med* **22**: 861-868.

Chujo T, Yamazaki T, Kawaguchi T, Kurosaka S, Takumi T, Nakagawa S, Hirose T. 2017. Unusual semi-extractability as a hallmark of nuclear body-associated architectural noncoding RNAs. *EMBO J* **36**: 1447-1462.

Evans RL, Park K, Turner RJ, Watson GE, Nguyen HV, Dennett MR, Hand AR, Flagella M, Shull GE, Melvin JE. 2000. Severe impairment of salivation in Na+/K+/2Cl- cotransporter (NKCC1)-deficient mice. *J Biol Chem* **275**: 26720-26726.

Fox AH, Nakagawa S, Hirose T, Bond CS. 2018. Paraspeckles: Where Long Noncoding RNA Meets Phase Separation. *Trends Biochem Sci* **43**: 124-135.

Hirose T, Virnicchi G, Tanigawa A, Naganuma T, Li R, Kimura H, Yokoi T, Nakagawa S, Benard M, Fox AH et al. 2014. NEAT1 long noncoding RNA regulates transcription via protein sequestration within subnuclear bodies. *Mol Biol Cell* **25**: 169-183.

Imamura K, Imamachi N, Akizuki G, Kumakura M, Kawaguchi A, Nagata K, Kato A, Kawaguchi Y, Sato H, Yoneda M et al. 2014. Long noncoding RNA NEAT1-dependent SFPQ relocation from promoter region to paraspeckle mediates IL8 expression upon immune stimuli. *Mol Cell* **53**: 393-406.

Inui M, Miyado M, Igarashi M, Tamano M, Kubo A, Yamashita S, Asahara H, Fukami M, Takada S. 2014. Rapid generation of mouse models with defined point mutations by the CRISPR/Cas9 system. *Sci Rep* **4**: 5396.

Kawaguchi T, Tanigawa A, Naganuma T, Ohkawa Y, Souquere S, Pierron G, Hirose T. 2015. SWI/SNF chromatin-remodeling complexes function in noncoding RNA-dependent assembly of nuclear bodies. *Proc Natl Acad Sci U S A* **112**: 4304-4309.

Kawai S, Takagi Y, Kaneko S, Kurosawa T. 2011. Effect of three types of mixed anesthetic agents alternate to ketamine in mice. *Exp Anim* **60**: 481-487.

Li R, Harvey AR, Hodgetts SI, Fox AH. 2017. Functional dissection of NEAT1 using

genome editing reveals substantial localization of the NEAT1_1 isoform outside paraspeckles. *RNA* **23**: 872-881.

Long Y, Wang X, Youmans DT, Cech TR. 2017. How do lncRNAs regulate transcription? *Sci Adv* **3**: eaao2110.

Mello SS, Sinow C, Raj N, Mazur PK, Bieging-Rolett K, Broz DK, Imam JFC, Vogel H, Wood LD, Sage J et al. 2017. Neat1 is a p53-inducible lincRNA essential for transformation suppression. *Genes Dev* **31**: 1095-1108.

Mito M, Kawaguchi T, Hirose T, Nakagawa S. 2016. Simultaneous multicolor detection of RNA and proteins using super-resolution microscopy. *Methods* **98**: 158-165.

Modic M, Grosch M, Rot G, Schirge S, Lepko T, Yamazaki T, Lee FCY, Rusha E, Shaposhnikov D, Palo M et al. 2019. Cross-Regulation between TDP-43 and Paraspeckles Promotes Pluripotency-Differentiation Transition. *Mol Cell* **74**: 951-965 e913.

Montgomery RK, Breault DT. 2008. Small intestinal stem cell markers. *J Anat* **213**: 52-58.

Moor AE, Harnik Y, Ben-Moshe S, Massasa EE, Rozenberg M, Eilam R, Bahar Halpern K, Itzkovitz S. 2018. Spatial Reconstruction of Single Enterocytes Uncovers Broad Zonation along the Intestinal Villus Axis. *Cell* **175**: 1156-1167 e1115.

Naganuma T, Nakagawa S, Tanigawa A, Sasaki YF, Goshima N, Hirose T. 2012. Alternative 3'-end processing of long noncoding RNA initiates construction of nuclear paraspeckles. *EMBO J* **31**: 4020-4034.

Nakagawa S, Naganuma T, Shioi G, Hirose T. 2011. Paraspeckles are subpopulation-specific nuclear bodies that are n16239143 19716791 25792598ot essential in mice. *J Cell Biol* **193**: 31-39.

Nakagawa S, Shimada M, Yanaka K, Mito M, Arai T, Takahashi E, Fujita Y, Fujimori T, Standaert L, Marine JC et al. 2014. The lncRNA Neat1 is required for corpus luteum formation and the establishment of pregnancy in a subpopulation of mice. *Development* **141**: 4618-4627.

Nakagawa S, Yamazaki T, Hirose T. 2018. Molecular dissection of nuclear paraspeckles: towards understanding the emerging world of the RNP milieu. *Open Biol* **8**.

Saha S, Murthy S, Rangarajan PN. 2006. Identification and characterization of a virus-inducible non-coding RNA in mouse brain. *J Gen Virol* **87**: 1991-1995.

Sasaki YT, Ideue T, Sano M, Mituyama T, Hirose T. 2009. MENepsilon/beta noncoding RNAs are essential for structural integrity of nuclear paraspeckles. *Proc Natl Acad Sci U S A* **106**: 2525-2530.

Schwab ME, Stockel K, Thoenen H. 1976. Immunocytochemical localization of nerve growth factor (NGF) in the submandibular gland of adult mice by light and electron microscopy. *Cell Tissue Res* **169**: 289-299.

Shelkovnikova TA, Robinson HK, Troakes C, Ninkina N, Buchman VL. 2014. Compromised paraspeckle formation as a pathogenic factor in FUSopathies. *Hum Mol Genet* **23**: 2298-2312.

Souquere S, Beauclair G, Harper F, Fox A, Pierron G. 2010. Highly ordered spatial organization of the structural long noncoding NEAT1 RNAs within paraspeckle nuclear bodies. *Mol Biol Cell* **21**: 4020-4027.

Wang Y, Hu SB, Wang MR, Yao RW, Wu D, Yang L, Chen LL. 2018. Genome-wide screening of NEAT1 regulators reveals cross-regulation between paraspeckles and mitochondria. *Nat Cell Biol* **20**: 1145-1158.

West JA, Mito M, Kurosaka S, Takumi T, Tanegashima C, Chujo T, Yanaka K, Kingston RE, Hirose T, Bond C et al. 2016. Structural, super-resolution microscopy analysis of paraspeckle nuclear body organization. *J Cell Biol* **214**: 817-830.

Wilusz JE, JnBaptiste CK, Lu LY, Kuhn CD, Joshua-Tor L, Sharp PA. 2012. A triple helix stabilizes the 3' ends of long noncoding RNAs that lack poly(A) tails. *Genes Dev* **26**: 2392-2407.

Yamazaki T, Souquere S, Chujo T, Kobelke S, Chong YS, Fox AH, Bond CS, Nakagawa S, Pierron G, Hirose T. 2018. Functional Domains of NEAT1 Architectural lncRNA Induce Paraspeckle Assembly through Phase Separation. *Mol Cell* **70**: 1038-1053 e1037.

Figure legends

Figure. 1 Generation of Neat1 □PAS mouse

(A) Schematics of gRNAs targeting the region surrounding the polyadenylation (poly-A) signal (PAS) AATAAA. Arrowheads indicate the positions of the primers used for the T7 endonuclease assay. (B) A T7 endonuclease assay evaluated the efficiency of the gRNA-Cas9 endonuclease activity. Note that gRNA #1 exhibited the highest activity. (C) Sequences analysis of genome-edited mice. 6 different mutant alleles were observed. The arrowhead indicates the position of the predicted cleavage site. Bold characters indicate the mutated nucleotides. (D) Comparison of the ratio of Neat1_1 and Neat1_2 expression in mutant alleles. Total RNAs was obtained from the salivary glands of mutant mice and Neat1 expression was analyzed by RT-qPCR. Note that 39del (hereafter Neat1 ΔPAS) exhibited the highest Neat1_2/Neat1_1 ratio. (E) An agarose electrophoresis gel image of PCR products that were amplified with genotyping primers. Note that a heteroduplex band that exhibited lower mobility was obtained from a heterozygous mouse (arrowhead). (F) Northern blot analyses of total RNAs obtained from mouse embryonic fibroblast (MEF) cells derived from wild-type (WT) and Neat1 ΔPAS (ΔPAS) mice. Neat1_1 was completely absent, whereas Neat1_2 was upregulated in Neat1 ΔPAS mice. (G) Simultaneous detection of Neat1_2 and Nono in MEF cells prepared from WT and ΔPAS embryos. Scale bar, 10 μm. Note that the number of paraspeckles increased in KO MEFs. (H) Quantification of the area of the paraspeckles shown in F, as visualized by violin/beeswarm plots. P values were calculated by a Student's t-test.

Figure 2. Northern blot analyses of Neat1 expression in various tissues of Neat PAS KO mice

(A) Schematics of probes used for the detection of Neat1_1 and Neat1_2. The Neat1/2 probe detected both isoforms, whereas the Neat1_2 probe targeted a region specific to the long isoform. (B, C) Expression of Neat1 isoforms, as revealed by probes that detected Neat1/2 (B) and Neat1_2 (C). Note the complete loss of Neat1_1 signals in all tissues and the variable upregulation of Neat1_2 in each tissue. The Neat1_1/2 probe failed to detect the upregulation of Neat1_2 in certain tissues for unknown technical

reasons. The liver expresses only Neat1_2, whereas the salivary gland expresses mostly Neat1_1. (D) Quantification of the results shown in B and C. The expression of Neat1_2 was quantified using the data shown in C and its biological replicates.

Figure 3. In situ hybridization analyses of Neat1 expression in Neat1 ΔPAS mice

(A-C) Expression of the Neat1 isoform revealed by probes that detected Neat1_1/2 and Neat1_2 in the intestine (A), liver (B), and salivary gland (C). Neat1_2 expression is normally restricted to the tip cells of the intestinal epithelium and expanded to the middle area of the epithelium in ΔPAS mice. Signals detected by the Neat1_1/2 probe were dramatically reduced in the salivary gland. None of these tissues exhibited histological abnormalities, as revealed by Haematoxylin-eosin staining (HE). Scale bars, 100 μm.

Figure 4. Simultaneous detection of Neat1_2 and the paraspeckle markers Sfpq and Nono in Neat1 ΔPAS mice

(A, B) Expression of Neat1_2 in the tip cells of the intestinal epithelium (top), the middle regions of the intestinal epithelium (middle), the liver, and the salivary gland, as revealed by probes that specifically detected Neat1_2 and by the simultaneous detection of the paraspeckle markers Sfpq (A) and Nono (B). Note the marked increase in paraspeckle formation, which was identified by accumulation of Sfpq and Nono, in the tip cells of the intestine epithelium and the liver cells. On the other hand, Neat1_2 accumulation was not always accompanied by the accumulation of paraspeckle markers in the granular duct cells. (C) Quantification of the paraspeckle area per cell in the tip cells in the intestinal epithelium, the middle of the intestinal epithelium, the liver, and granular duct cells in the salivary gland. Note that the majority of the granular duct cells did not form paraspeckles in the wild-type (WT) mice. (D) Simultaneous detection of Neat1_2 and Nono at higher magnification, using structural illumination microscopy. Scale bars, 10 μm in A and B, and 1 μm in D.

Figure 5. Expression of paraspeckle proteins in the intestine, liver, and salivary gland

(A) Immunohistochemical detection of Category 1A (Sfpq, Nono, and Hnrnpk),

Category 1B (Fus, Brg1), Category 2 (Tardbp), Category 3A (Cpsf6), and Category 3B (Pspc1, Ewsr1) paraspeckle proteins (green) in the intestinal epithelium, liver, and granular duct cells in the salivary gland. DAPI-stained nuclei are shown in magenta. Note that the paraspeckle proteins did not exhibit clear paraspeckle localization here because of the intense nucleoplasmic signals, which were reduced after harsh in situ hybridization treatments that extracted weakly-fixed free proteins in the nucleoplasm (West et al. 2016). These paraspeckle proteins were ubiquitously expressed in the intestine and liver, while the granular duct cells expressed much lower levels of Brg1, Hnrnpk, Fus, Pspc1, and Ersr1. The arrowhead in the Hnrnk/salivary gland panel indicates the intense signals observed in acinar cells in the salivary gland. Scale bar, 10 µm. (B) Summary of the expression shown in (A). (C) Detection of paraspeckle proteins in Western blots. Note that all of these proteins migrated to the same positions, while the expression levels were different. Arrowheads indicate endogenous immunoglobulin bands detected with the anti-mouse secondary antibodies.

Figure 6. Expression patterns of marker genes were not significantly altered in the intestine and salivary gland in Neat1 ΔPAS mice

(A) Schematics of the expression patterns of marker genes expressed in the intestinal epithelium. Note that the zonation of the enterocytes can be discriminated by different combinations of the marker genes. (B) In situ hybridization analyses of marker genes in the intestine. (E) Schematics of the expression pattern of the acinar cell marker *Nkcc1* and the granular duct cell marker *Ngf*. (F) In situ hybridization analyses of marker genes in the salivary gland. Scale bars, 100 µm.

Isobe et al., Figure 1

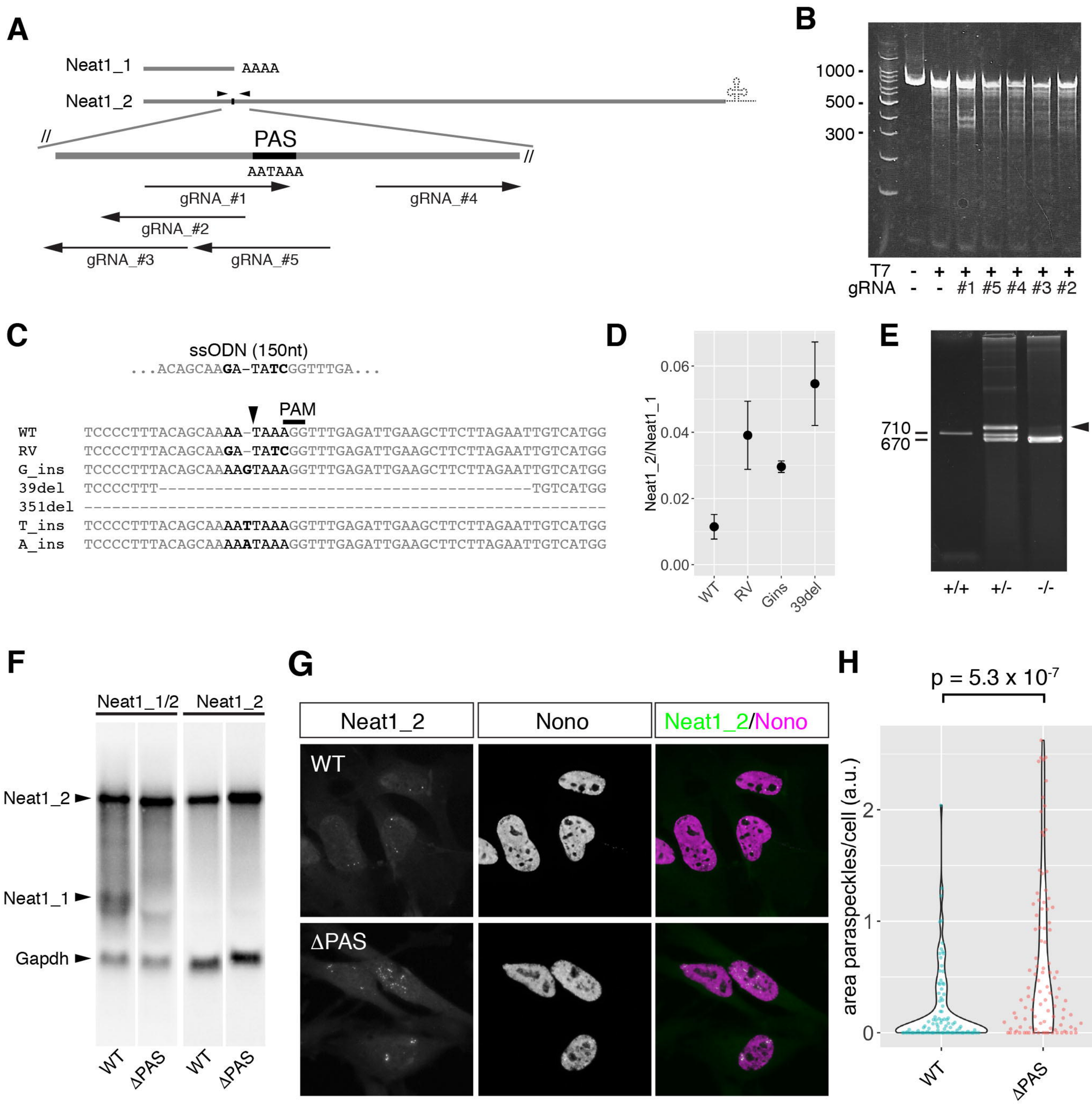

Isobe et al. Figure 2

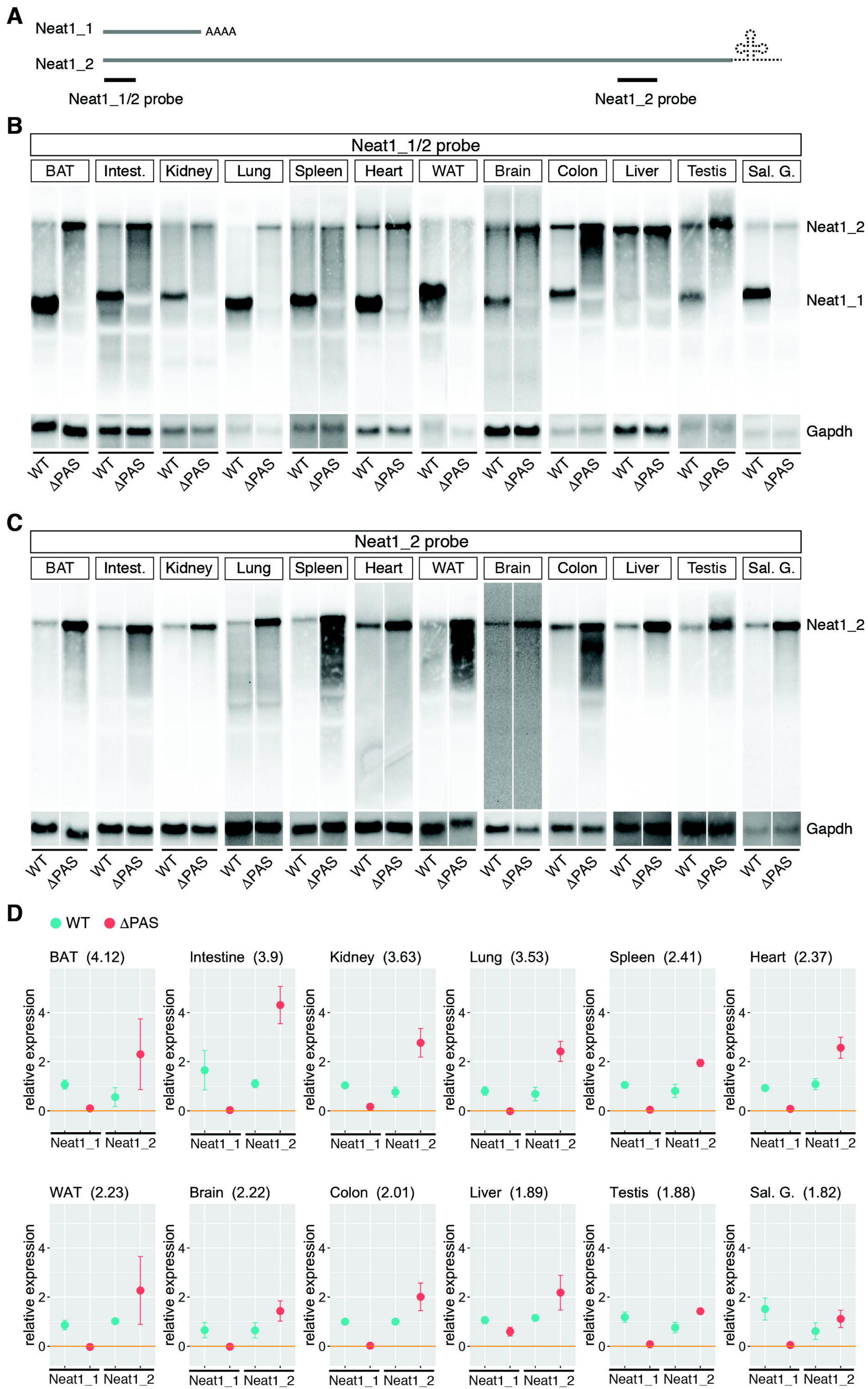

Isobe et al. Figure 3

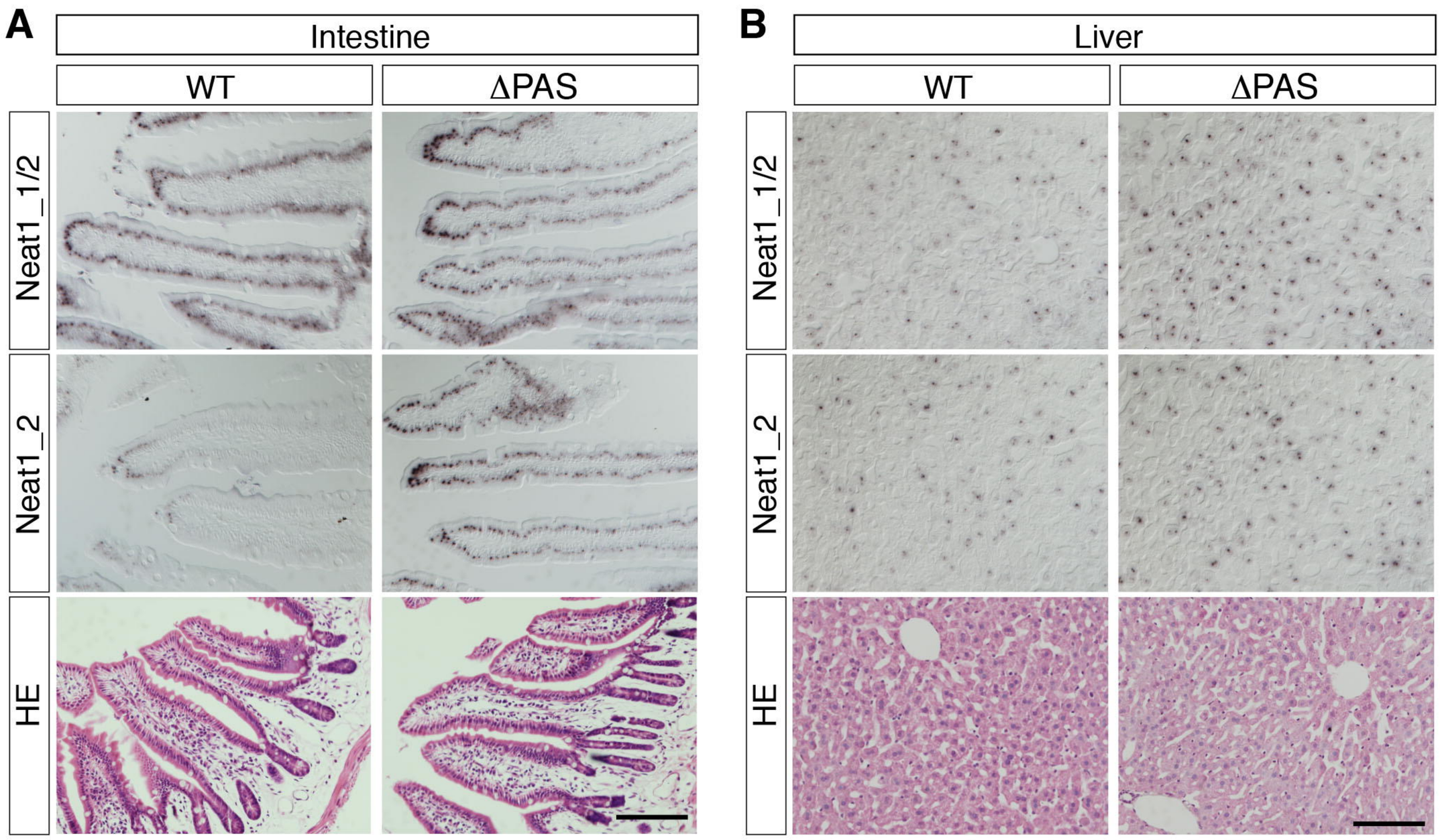

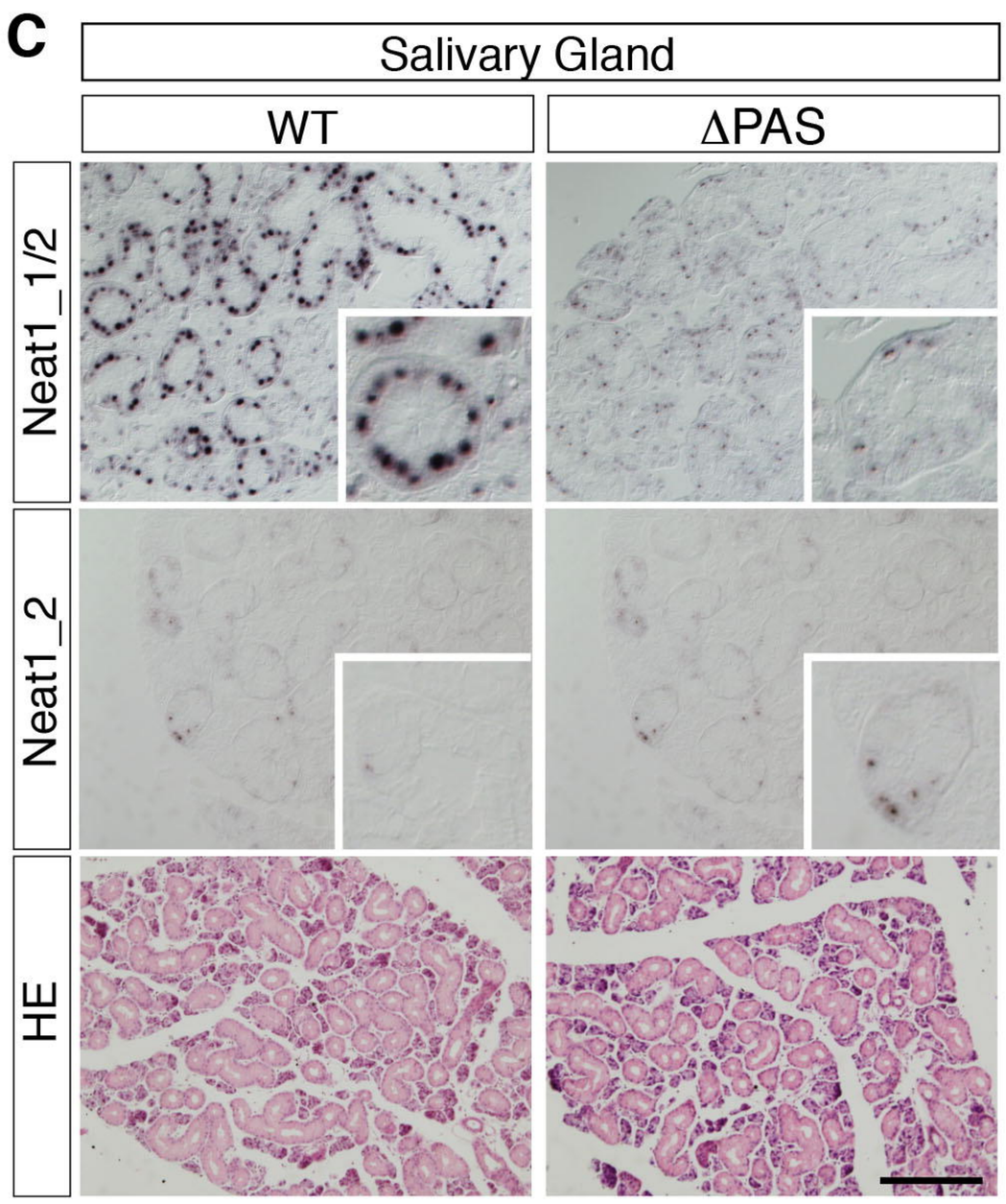

Isobe et al. Figure 4

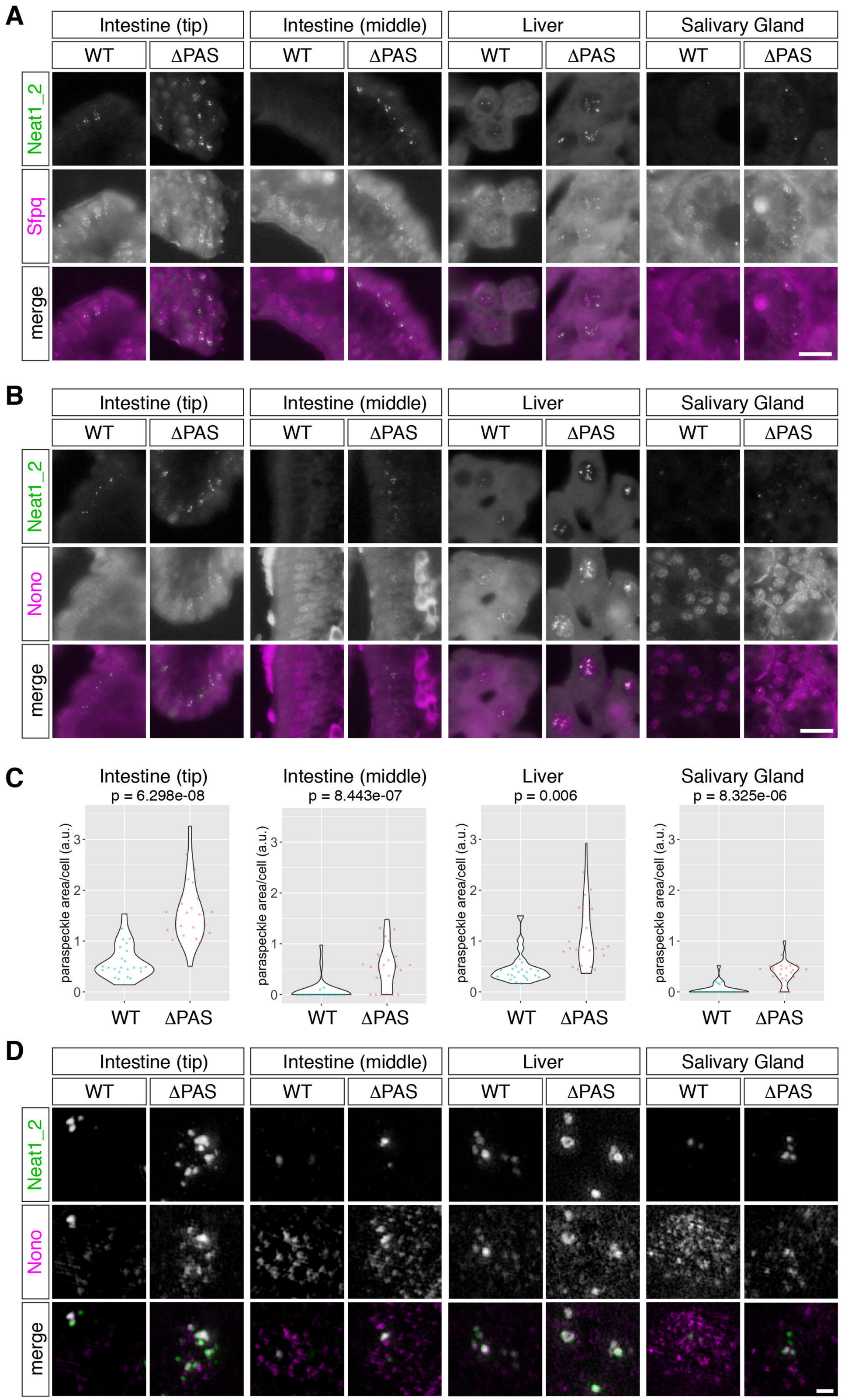

Isobe et al. Figure 5

A

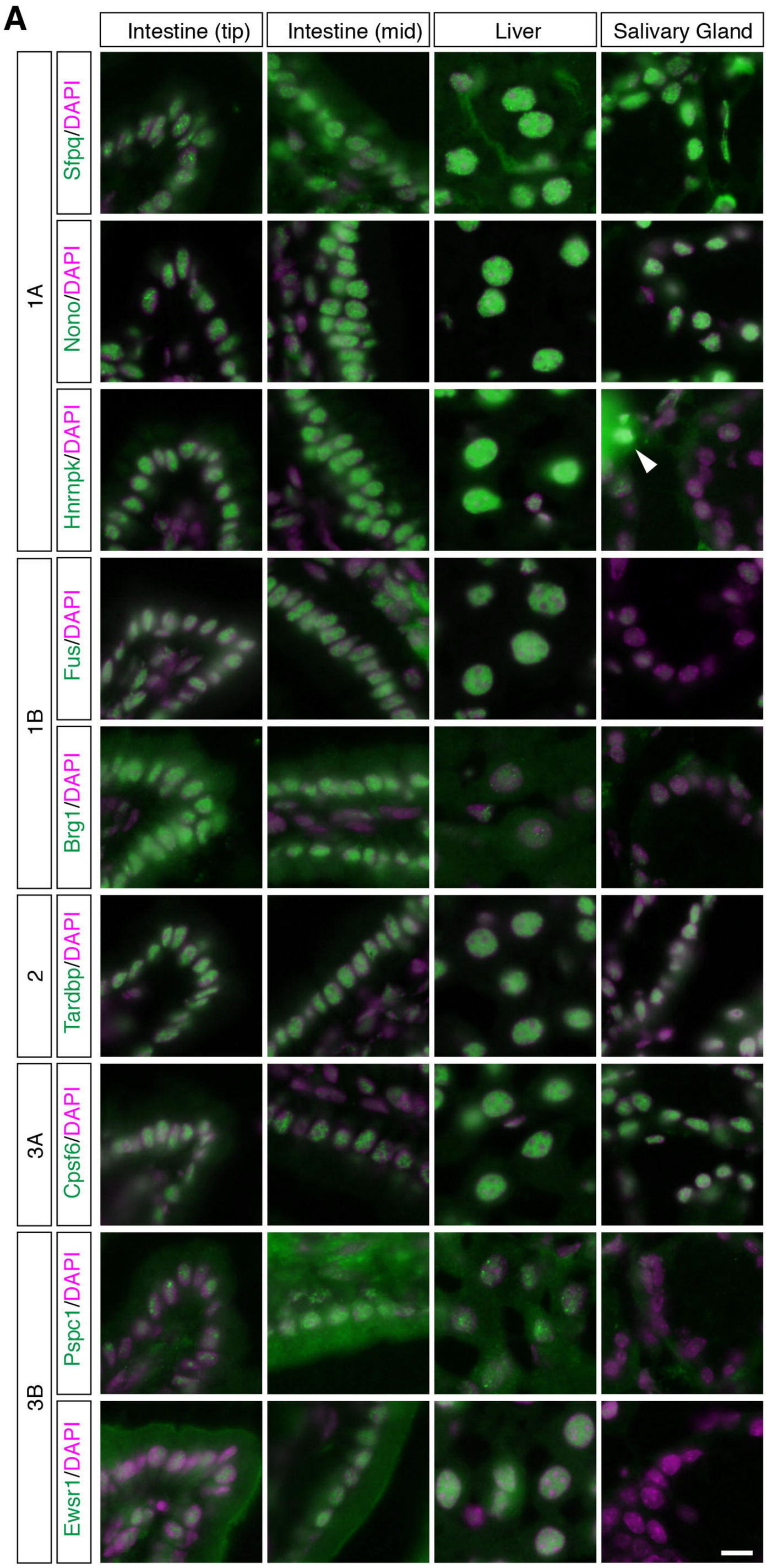

B

	Intestine (tip)	Intestine (middle)	Liver	Salivary (GD)
Sfpq	+++	+++	+++	+++
Nono	+++	+++	+++	+++
HnrnpK	+++	+++	+++	+/-
Fus	+++	+++	+++	+
Brg1	+++	+++	+	+
Tardbp	+++	+++	+++	+++
Cpsf6	+++	+++	+++	+++
Pspc1	+++	+++	+++	-
Ewsr1	++	+++	+++	-

C

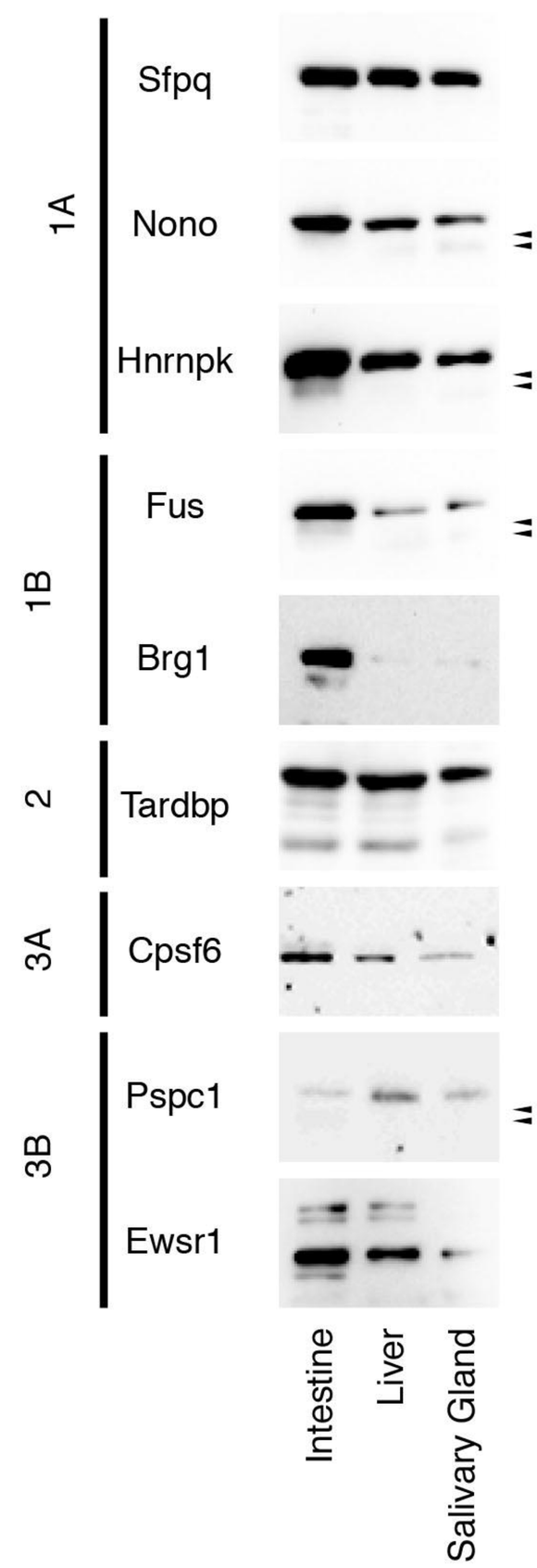
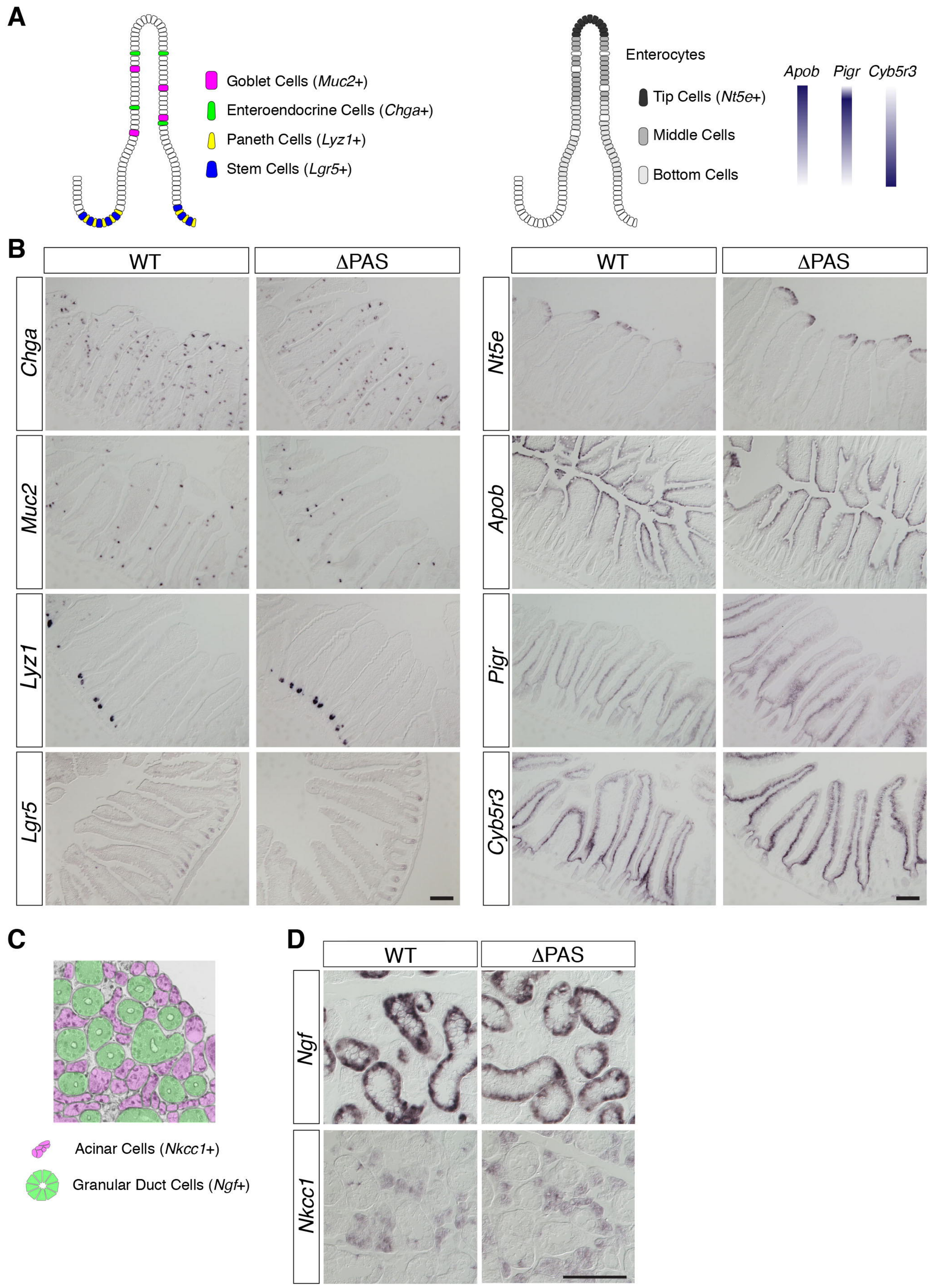
Isobe et al. Figure 6